PCCP

The Roles of Surface Structure, Oxygen Defects, and Hydration in the Adsorption of CO_2 on Low-Index $ZnGa_2O_4$ Surfaces: A First-Principles Investigation

Chuanyi Jia [a,b)], Weiliu Fan [a)] [*], Xiufeng Cheng [b)], Xian Zhao [b)], Honggang Sun [b)], Pan Li [b)], and Na Lin [b)]

a) School of Chemistry and Chemical Engineering, Shandong University, Jinan 250100 China

b) State Key Laboratory of Crystal Materials, Shandong University, Jinan 250100 China

ABSTRACT: The effects of the surface atomic and electronic structure, oxygen defects, and hydration on CO_2 adsorption on $ZnGa_2O_4$ (100), (110), and (111) surfaces was studied using density functional theory (DFT) slab calculations. For the perfect (100) surface, the most stable adsorption state involved the Zn–O–Ga bridge site, with an adsorption energy of 0.16 eV. In the case of the (110) and (111) surfaces, the strongest binding occurred on the Zn–O bridge sites, with much lower adsorption energies of -0.22 eV and -0.35 eV, respectively. In addition, the perfect surfaces showed CO_2 activation ability, but dissociation adsorption could not proceed. The oxygen vacancies on these three surfaces (1) made the metal sites beside them carry less positive charge and further reduced the adsorption energies on these metal sites, and (2) created efficient adsorption sites that allowed even dissociative adsorption. The most favorable molecular and dissociative adsorption states both involved the O_{3c} vacancy site of the (100) surface, and these two processes were spontaneous with adsorption energies of 0.74 eV and 0.80 eV, respectively. When H_2O molecules are

---

[*] To whom all correspondences should be addressed. Tel: 86-531-88366330, Fax: 86-531-88364864, E-mail: fwl@sdu.edu.cn.

present on the perfect and defective surfaces, the generation of hydrogen bonds between H_2O and CO_2 would slightly enhance the stability of adsorption (except for that on the **(111)-Vo$_{3c}$** surface), making it energetically favorable. However, the co-adsorption of H_2O could also increase the energy barriers for the decomposition reactions on the defective surfaces, making them kinetically unfavorable. Furthermore, the oxygen vacancy defects showed good activity for H_2O adsorption and decomposition, as well. Thus, when H_2O and CO_2 were both present in the adsorption system, H_2O would compete with CO_2 for the oxygen vacancy sites and further decrease the amount of CO_2 adsorption and decomposition. These findings have important implications regarding the decomposition of CO_2 on the $ZnGa_2O_4$ surfaces and can provide theoretical guidance for chemists to efficiently synthesize $ZnGa_2O_4$ catalysts.

1. INTRODUCTION

With the increasing greenhouse effect and energy crises,[1-3] there has been increased interest in the development of environmentally clean and safe processes that can be used to expand our energy infrastructure. Because CO_2 produced by human activities is the chief greenhouse gas, it will be of great concern to find a way to remove this compound from the atmosphere. Therefore, there is considerable impetus to investigate the potential usefulness of carbon dioxide as a reactant in hydrocarbon synthesis.

Recently, researchers have studied the conversion of CO_2 over various modified or

unmodified forms of catalysts,[4-7] among which semiconductor photocatalysts have got much attention for their potential applications in green energy and environmental cleanup.[8-12] It have been three decades since photocatalytic reduction of CO_2 to formic acid, formaldehyde, methanol, and methane as the main products was first demonstrated.[13] From then on, many efforts have been devoted to developing efficient photocatalysts for the reduction of CO_2. The structure dependence of the reaction rates and the selectivity of heterogeneous catalytically active sites are growing into new popular fields of study.[14,15] Moreover, surface defects and hydration are often considered to be important for heterogeneous catalysis as well, since these particular factors also play important roles in the reactant-surface binding and the formation of bonds between the surface atoms and CO_2 molecules.[16-20] However, many of the previous studies were focused on the addition of transition metals or co-catalysts to improve the catalytic efficiency.[21-27] The morphology, defects, and hydration of the catalyst, however, have rarely been considered. To gain more understanding of the influences of these factors, we need to carry out further research to determine the relationship between the microstructure and reaction activity of the catalysts.

As a typical ternary oxide, zinc gallate ($ZnGa_2O_4$) has good activity for water splitting, pollutants degradation, and so on.[28-32] Recently, well-designed $ZnGa_2O_4$ catalysts were also found to show good photocatalytic activity for the reduction of CO_2 to renewable hydrocarbon fuel (CH_4) in the presence of water vapor.[33] Therefore, the interaction of CO_2 with $ZnGa_2O_4$ surfaces is a subject of great interest, not only for fundamental research but also for industrial engineering. However, because of the

great complexity of the $ZnGa_2O_4$ surface structure, a clear and general picture of the

interaction between CO_2 molecules and the $ZnGa_2O_4$ surfaces is not yet available.

Moreover, some former studies indicated that dissociative adsorption, $CO_2 \rightarrow CO + O$,

was particularly crucial for the process of CO_2 decomposition.[34-38] Therefore,

identifying the reaction mechanisms (especially the mechanism of dissociative

adsorption) and the effect of the surface structure, defects, and hydration on CO_2

activation and decomposition will have important implications regarding the

photoreduction of CO_2 on $ZnGa_2O_4$ catalysts.

In our present work, the structure sensitivity and the effects of the oxygen

vacancy defects and hydration of $ZnGa_2O_4$ catalysts were studied by comparing the

adsorption of CO_2 on the perfect, reduced, and hydrated (100), (110), and (111)

surfaces of low-index $ZnGa_2O_4$. The majority of this work is aimed at gaining a

theoretical understanding of the CO_2 adsorption on the $ZnGa_2O_4$ surfaces and of the

detailed chemistry occurring on its surfaces.

COMPUTATIONAL DETAILS AND MODELS

All calculations were performed in the framework of the periodic density functional

theory (DFT) by using code from the Cambridge Sequential Total Energy Package

(CASTEP).[39] The interactions between ion cores and valence electrons were dealt by

the ultrasoft pseudopotential[40]. For Zn, the $3d$ and $4s$ states were treated as valence

states, whereas for Ga, the $3d$, $4s$, and $4p$ states were treated as valence states. The

Perdew's and Wang's 1991 (PW91) functional within the generalized gradient

approximation (GGA)[41,42] was chosen to describe the exchange correlation energy.

The energy cutoff of the plane-wave basis set was chosen to be 300 eV to expand the Kohn-Sham wave functions for the valence electrons. The convergence test for the energy cutoff was shown in the Supporting Information (Figure S1). The Monkhorst–Pack grids of $2 \times 2 \times 1$ κ-point were used to cover the irreducible Brillouin zone (the test for the k-point for each surface was shown in Table S1). The maximum force for the convergence criteria of the structural optimization and energy calculation was chosen to be 0.05 eV/Å (our calculations indicated that smaller maximum force had little effect on the adsorption states, as shown in Table S2). For the self-consistent field (SCF), maximum stress and maximum displacement were separately chosen to be 2×10^{-6} eV/atom, 0.1 GPa and 2×10^{-3} Å.

Among the three low-index $ZnGa_2O_4$ surfaces, the (100) and (111) surfaces were modeled using a 2×2 supercell with dimensions of 11.97 Å $\times$ 11.97 Å $\times$ 27.50 Å and 11.97 Å $\times$ 11.97 Å $\times$ 29.16 Å, respectively. Sixteen $ZnGa_2O_4$ molecular units in each slab were distributed in seven layers. The supercell for the (110) surface included a 2×1 surface unit cell and six atomic layers with twelve molecular units, resulting in a supercell size of 8.46 Å $\times$ 11.97 Å $\times$ 27.62 Å. The vacuum regions separating the slabs were all set to widths of 20 Å, which is enough distance to screen the self-interaction effects of the periodic boundary conditions. On these three surfaces, the adsorbates (H_2O and CO_2) and all of the atoms in the three topmost layers were allowed to relax, whereas to simulate the bulk effects the rest layers in the bottom were fixed. To further observe the charge transfers and population analyses, we also performed the Mulliken populations on the equilibrium structure, which was carried out

by using a projection of the plane-wave states onto a linear combination of atomic

orbital basis sets.[43, 44]

The binding energies of the adsorbed CO_2 and H_2O are defined as

$$E_{ad}^{CO_2} = (E_{sur/CO_2} - E_{sur} - E_{CO_2}),$$

$$E_{ad}^{H_2O} = (E_{sur/H_2O} - E_{sur} - E_{H_2O})$$

where

E_{sur} is the total energy of the bare slab of the surface,

E_{CO_2} is the total energy of free CO_2,

E_{sur/CO_2} is the total energy of the slab with the adsorbed CO_2 molecule on the

surface,

E_{H_2O} is the total energy of free H_2O,

E_{sur/H_2O} is the total energy of the slab with the adsorbed H_2O molecule on the

surface.

This means that a positive E_{ad} value will lead to an exothermic adsorption

reaction. Moreover, in order to determine accurate activation barriers for the reaction,

we performed the complete LST/QST approach to search for transition states as well.

3. RESULTS AND DISCUSSION

3.1. CO_2 Adsorption on the Dry Perfect $ZnGa_2O_4$ (100), (110), and (111)

Surfaces. Firstly, we studied the adsorption of CO_2 on the dry perfect $ZnGa_2O_4$

surfaces. In Figure 1, it can clearly be seen that the Zn_{2c} (2-fold-coordinated Zn), Zn_{3c}

(3-fold-coordinated Zn), Ga_{3c} (3-fold-coordinated Ga), Ga_{4c} (4-fold-coordinated Ga),

and Ga_{5c} (5-fold-coordinated Ga) metal atoms on these three $ZnGa_2O_4$ surfaces were coordinately unsaturated and carried positive charges (seen in Figure 1). As pointed out in our previous work,[45] this would make them strong Lewis acids that can adsorb CO_2 by interacting with its O atoms,[46] whereas the surface O atoms (O_{3c} or O_{4c}),
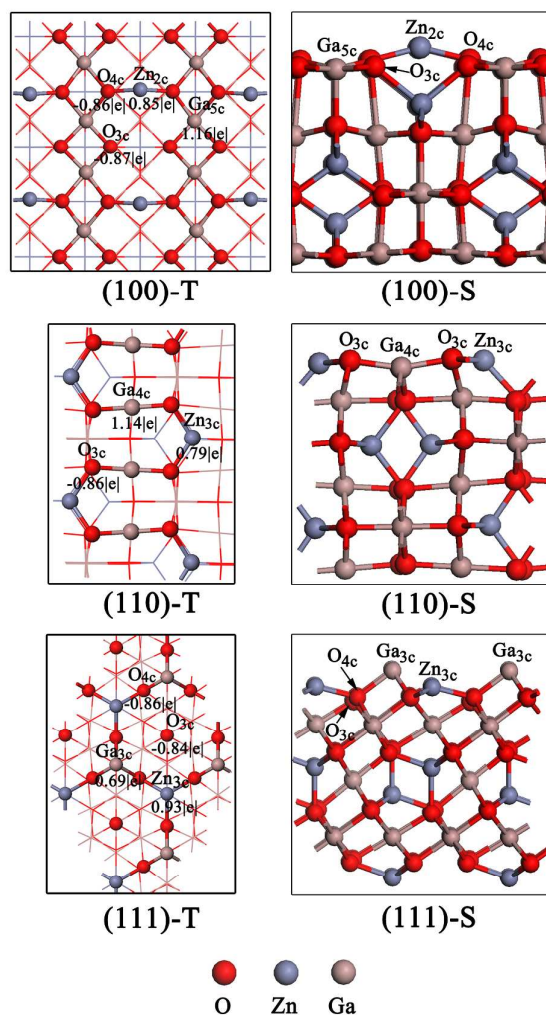

Figure 1. The top and side views of the optimized structures of the dry perfect $ZnGa_2O_4$ (100), (110) and (111) surfaces. The surface sites and Mulliken charges carried by them are labeled on each surface as well.

which carry negative charges, would be strong Lewis bases adsorbing the C atoms of CO_2. Moreover, because the surface structures and the charges carried by the surface

atoms were different from each other for the different surfaces, their adsorption behaviors would be different, as well. To further understand the correlation of the surface atomic and electronic structures with catalytic activity, detailed calculations and discussion of the interactions between CO_2 molecules and the surfaces of the $ZnGa_2O_4$ catalyst are presented in the flowing sections.

After considering all the possible adsorption states, we obtained five models of the interaction between CO_2 and the surface, as shown in Figure 2. In this paper, they are labeled as **(a)** CO_2 perpendicular to the surface, **(b)** only the C atom adsorbed on the surface metal atom to form a monodentate carbonate species, **(c)** both the O_a and C atoms interacting with the surface atoms to generate a bidentate carbonate species, **(d)** two O atoms of CO_2 binding with two metal atoms and the C atom binding with an O atom to form a bridge geometry, and **(e)** only the two O atoms of CO_2 binding with two metal atoms to form a bridge geometry. In these adsorption configurations, the two oxygen atoms of the adsorbed CO_2 are labeled as O_a and O_b if they were not in equivalent positions. Different sites on the perfect $ZnGa_2O_4$ surfaces, including Zn, Ga, Zn–O, Ga–O, Ga–Ga, and Zn–O–Ga sites, were examined for CO_2 adsorption. The results showed that the CO_2 molecule had a tendency to keep a linear structure when it interacted with the perfect $ZnGa_2O_4$ surfaces; if we put a bent structure on these surfaces, it would return to the linear structure after optimization.
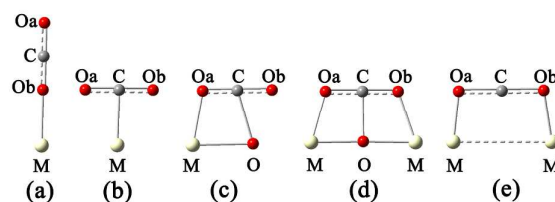

8

Figure 2. All the possible models of adsorbed CO_2 on the $ZnGa_2O_4$ surfaces.

Comparing the adsorption energies of all the sites on each surface, we found that the most stable ones were model **(d)** on the (100) surface (**100, Zn-Ga-d**), model **(c)** on the (110) surface (**110, Zn-c**), and model **(c)** on the (111) surface (**111, Zn-c**), as shown in Figure 3. The adsorption energies and key structural parameters of these three models are shown in Table 1, and the remaining less stable structures on each surface are provided in the Supporting Information (Figure S2-S4). For configuration (**100, Zn-Ga-d**), CO_2 was adsorbed across the Zn–O–Ga bridge site. The distances between O_b and Zn_{2c}, O_a and Ga_{5c}, and C and O_{4c} were 2.66 Å, 3.03 Å, and 3.13 Å, respectively. Therefore, both oxygen atoms and the carbon atom in CO_2 could interact with the surface, and all these interactions enhanced the stability of the adsorption state. Moreover, the main adsorption site Zn_{2c} on the (100) surface protruded above the surface, which could lead to steric hindrance preventing the CO_2 molecule form reaching the surface. However, for configurations (**110, Zn-c**) and (**111, Zn-c**), it can be seen that the main interactions between the CO_2 molecule and the surface happened between one oxygen atom of CO_2 and the surface Zn_{3c} atom, and these configurations were less stable than configuration (**100, Zn-Ga-d**), since the interactions were weaker. The stability of **Zn-Ga-d** adsorption on the (110) and (111)
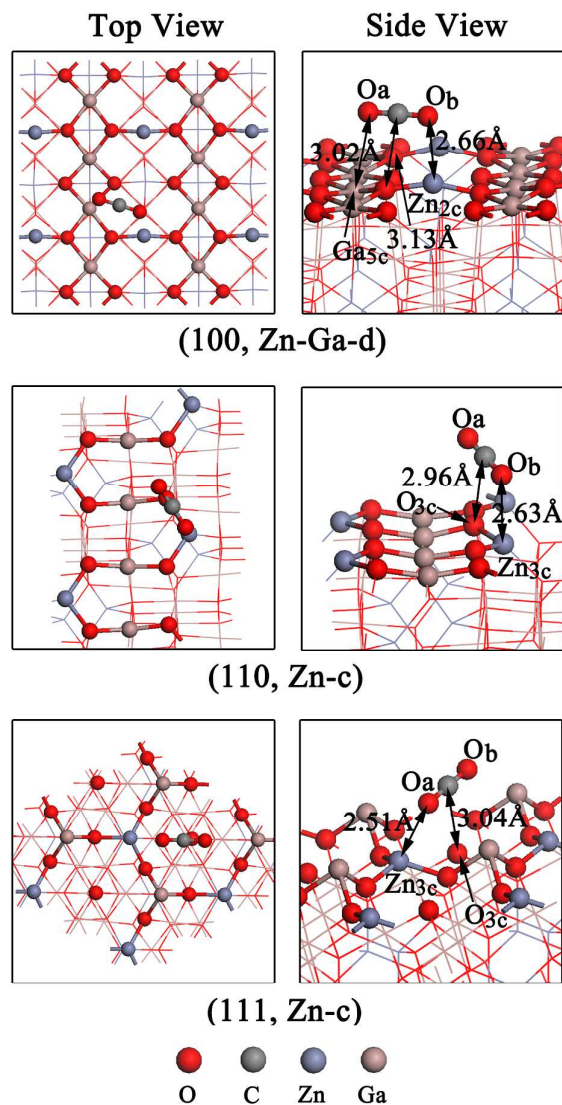
Figure 3. Top (left) and side (right) views of the most stable CO_2 molecular adsorption state on each surface. **(100, Zn-Ga-d)**: the CO_2 molecule adsorbed by the Zn and Ga sites on the (100) surface (the **d** adsorption type in Figure 2); **(110, Zn-c)**: the CO_2 molecule adsorbed by the Zn site on the (110) surface (the **c** adsorption type in Figure 2); **(111, Zn-c)**: the CO_2 molecule adsorbed by the Zn on the (111) surface (the **c** adsorption type in Figure 2).

Configurations	E_{ads} (eV)	$C-O_a$ bond(Å)	$C-O_b$ bond(Å)	O_a-C-O_b angle(°)	Charge($|e|$)			
					C	O_a	O_b	CO_2
(100,Zn-Ga-d)	-0.16	1.178	1.185	178.5	0.77	-0.42	-0.45	-0.10
(110,Zn-c)	0.22	1.176	1.185	178.8	0.78	-0.42	-0.46	-0.10
(111,Zn-c)	0.35	1.187	1.178	178.7	0.77	-0.47	-0.42	-0.12
CO_2-mol	—	1.180	1.180	180.0	1.00	0.50	0.50	0.00

Table 1. Structural Parameters, Adsorption Energies and Mulliken Charges of CO_2 Adsorbed in the Most Stable Configurations on Each Perfect $ZnGa_2O_4$ Surface.

surfaces was also calculated, as depicted in Figures S2 and S3. The reason that these two adsorption states are quite unstable is the specific atomic and electronic structures of these two surfaces. From Figures S2 and S3, we can see that the Ga_{4c} and Zn_{3c} atoms on the (110) surface are both located below the surface level, and similarly, the Zn_{3c} and O_{4c} atoms on the (111) surface are located below the surface level, as well. As such, the CO_2 molecules must overcome more steric hindrance to reach these surfaces, which would significantly reduce the strength of the interactions between the CO_2 molecules and the surface atoms. Moreover, the differences among the charges carried by the surface metal atoms are important reasons that the **Zn-Ga-d** adsorption on these two surfaces is less stable. As shown in Figure 1, the charges carried by Zn_{3c} and Ga_{4c} on the (110) surface were 0.79 $|e|$ and 1.14 $|e|$, respectively, which are less than the corresponding charges on the Zn_{2c} (0.85 $|e|$) and Ga_{5c} (1.16 $|e|$) atoms on the (100) surface. This means that the acidity of the metal atoms on the (110) surface is weaker than that on the (100) surface, which further made the adsorption on the (110)

11

surface less stable. For the (111) surface, although the charge on the Zn_{3c} (0.93 $|e|$)

atom was a little higher than the charge on the Zn_{2c} atom on the (100) surface, the

charge on the Ga_{3c} (0.69 $|e|$) was much less than that on the Ga_{5c} atom. Therefore, the

total interaction strengths between these two metal atoms on the (111) surface and the

CO_2 was less than those on the (100) surface.

The above results indicate that the surface atomic and electronic structure would

play an important role in the interaction between CO_2 and the $ZnGa_2O_4$ catalyst. The

adsorption energies of CO_2 on the (100), (110), and (111) surfaces were -0.16 eV, 0.22

eV, and 0.35 eV (seen in Table 1), respectively, which means that only CO_2 adsorption

on the (100) surface was exothermic and thermodynamically favorable. In addition,

the perfect $ZnGa_2O_4$ surfaces showed CO_2 activation ability, but the CO_2 molecule

could not decompose on them. Therefore, there must be other factors that have

obvious effects on CO_2 adsorption and activation, among which the oxygen vacancy

(Vo) defects and hydration are considered as common factors here.

Oxygen vacancy is an intrinsic defect in metal oxides, and it usually shows good

activity for CO_2 adsorption, as shown by many experimental and theoretical

studies.[47-49] Meanwhile, when water is adsorbed on the metal oxide surface it can

significantly influence the nature of the surface sites and further affects the

subsequent adsorption and decomposition of CO_2 molecules as well.[19] Thus, in the

following two sections we further discuss the effect of oxygen vacancy and hydration

on CO_2 adsorption and decomposition on $ZnGa_2O_4$ (100), (110), and (111) surfaces.

3.2. CO_2 Adsorption and Dissociation on Dry (100), (110), and (111) Surfaces

with Oxygen Vacancy Defects. In this section, we further explore the CO_2 adsorption on the dry $ZnGa_2O_4$ surfaces with oxygen vacancy defects. As shown in Figure 4, there is a total of five kinds of oxygen vacancy defects on these three surfaces: O_{3c} and O_{4c} vacancies on the (100) surface, an O_{3c} vacancy on the (110) surface, and O_{3c} and O_{4c} vacancies on the (111) surface. Our previous study showed that the generation of oxygen vacancy defects causes significant charge redistribution that reduces the positive charges carried by the metal atoms beside them as compared to those on clean surfaces.[45] This change would decrease the acidity of these metal atoms and further decrease the stability of the adsorption states of CO_2 on these sites. In the following sections, we would discuss in detail the changes in the adsorption behavior on the defective (100), (110), and (111) surfaces.

$$(100) \qquad (110) \qquad (111)$$
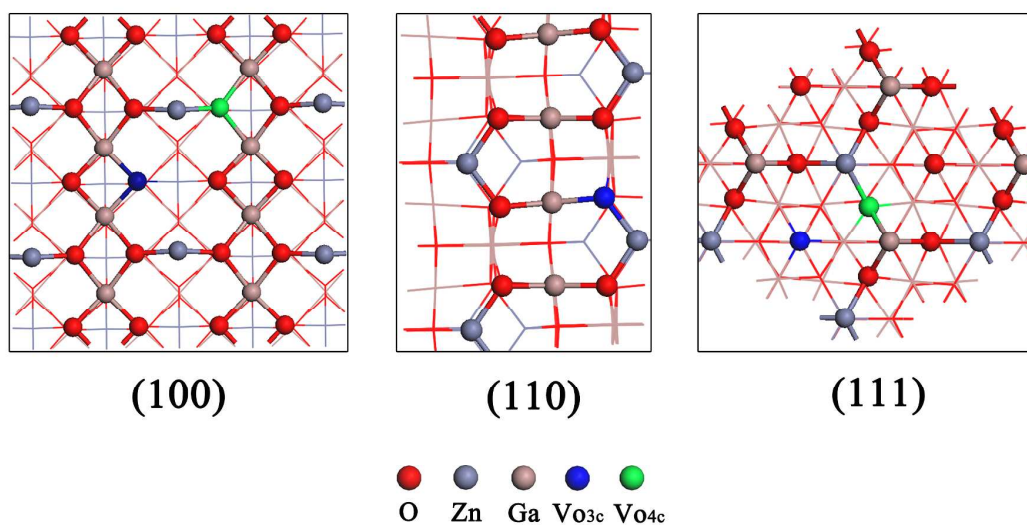
O   Zn   Ga   Vo3c   Vo4c

Figure 4. All the possible oxygen vacancy defects on the (100), (110) and (111) surfaces.

Firstly, we compared all of the adsorption energies of different configurations in the presence of an oxygen vacancy defect (Vo_{3c} or Vo_{4c}) on the (100) surface and obtained

the most stable configurations, as shown in Figure 5. We found that when such a surface vacancy presented on the surface, it could modify the energy for configurations in which CO_2 is adsorbed on the perfect surface at the sites near the vacancy. The presences of an oxygen vacancy defect will significant decrease the adsorption energies as well (Figure 5, **(100-Vo₃c, Zn-Ga-d)** and **(100-Vo₄c, Zn-Ga-d)**). This can be explained by the decrease in the charges on the metal atoms near the vacancy, which would decrease the acidity of the metal atoms. Moreover, we also found that the O_{3c} vacancy was an active site for CO_2 adsorption (Figure 5-**(100-Vo₃c-mol)**) and decomposition (Figure 5-**(100-Vo₃c-dis)**). The adsorption
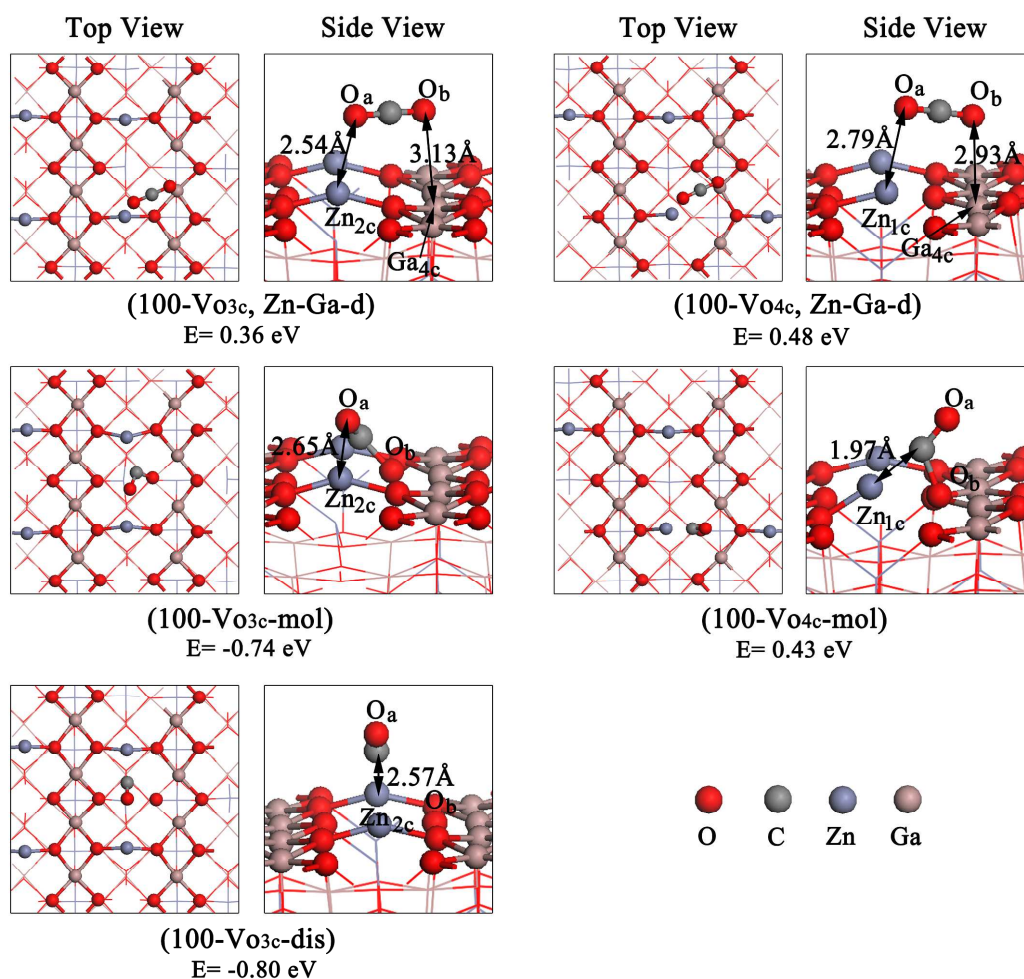

Figure 5. Top (left) and side (right) views of CO_2 adsorption structures and energies

14

on O_{3c} and O_{4c} vacancy defective $ZnGa_2O_4$ (100) surface. **(100-Vo$_{3c}$, Zn-Ga-d)**: the CO_2 molecule adsorbed by the Zn and Ga sites on the **(100)-Vo$_{3c}$** surface (similar to **(100, Zn-Ga-d)** state in Figure 3); **(100-Vo$_{3c}$-mol)**: the molecular adsorption on the oxygen vacancy site of the **(100)-Vo$_{3c}$** surface; **(100-Vo$_{3c}$-dis)**: the dissociative adsorption on the oxygen vacancy site of the **(100)-Vo$_{3c}$** surface; **(100-Vo$_{4c}$, Zn-Ga-d)**: the CO_2 molecule adsorbed by the Zn and Ga sites on the **(100)-Vo$_{4c}$** surface (similar to **(100, Zn-Ga-d)**) state in Figure 3); **(100-Vo$_{4c}$-mol)**: the molecular adsorption on the oxygen vacancy site of the **(100)-Vo$_{4c}$** surface.

energies of these two configurations were both much higher than those of the other sites on the defective or perfect surfaces (Figure 3 and 5). This suggests that the generation of O_{3c} vacancy defects could promote CO_2 adsorption and decomposition on the (100) surface. Because dissociative adsorption has a higher adsorption energy than molecular adsorption, dissociative adsorption on the **(100)-Vo$_{3c}$** surface would be more favorable thermodynamically. On the **(100)-Vo$_{4c}$** surface, the molecular adsorption state on the O_{4c} vacancy site, however, was quite unstable because of the large steric hindrance caused by the Zn and Ga atoms near the vacancy, and dissociative adsorption could not occur on this surface. In fact, our calculation indicated that the CO_2 molecule tended to stay far away from the surface rather than dissociate on it. Thus, the **(100)-Vo$_{4c}$** surface would not be a good surface for CO_2 adsorption and decomposition. For the defective (110) and (111) surfaces, a detailed discussion was performed in the Supporting Information. We found that the molecular adsorption on the oxygen vacancy site is much easier to happen than the dissociative

adsorption on the **(110)-O$_{3c}$**, **(111)-O$_{3c}$**, and **(111)-O$_{4c}$** surfaces, and the dissociative

adsorption states are all less stable than the state on the **(100)-O$_{3c}$** surface as well.

Therefore, compared to the **(100)-O$_{3c}$** surface, CO$_2$ decomposition on these three

surfaces would be less favorable thermodynamically.

   Having studied the favorable dissociated structures, we now turn to exploring the

dissociative adsorption mechanism of CO$_2$ on the defective surfaces. The potential

energy profiles and the structures of the transition states are both shown in Figure 6.

For the reaction process on the **(110)-Vo$_{3c}$** surface, the molecularly adsorbed CO$_2$

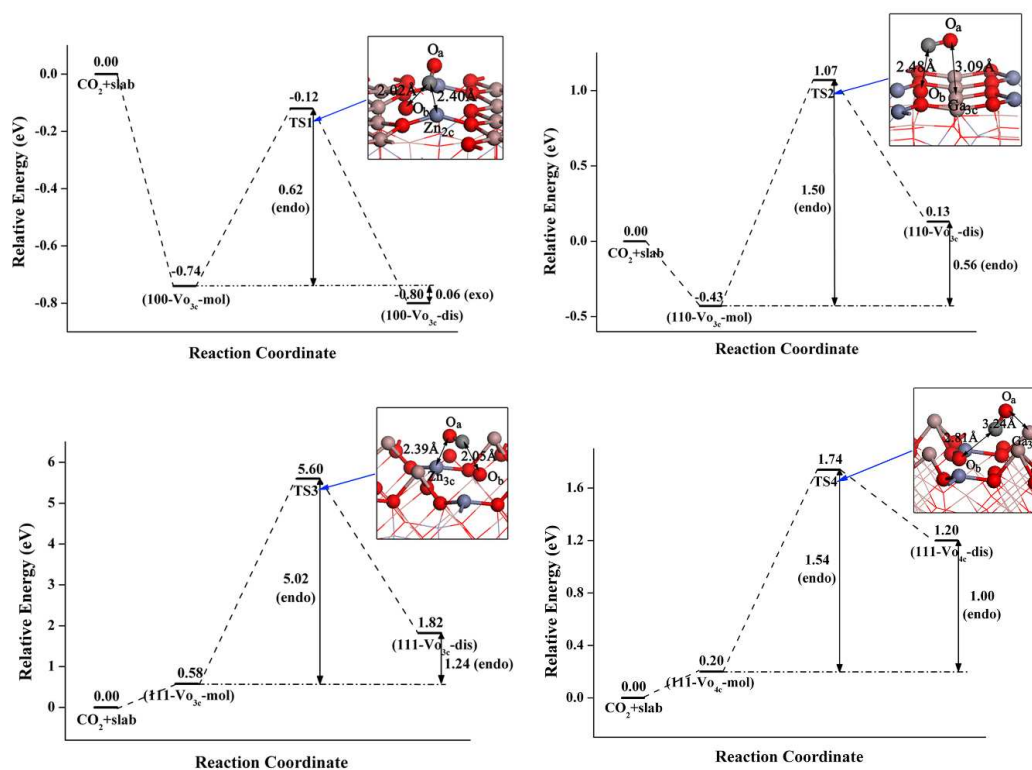dissociated into adsorbed CO$_a$ and O$_b$ atoms through a transition state TS1, with an

Figure 6. Potential energy profiles for the dissociation of CO$_2$ on the O$_{3c}$ or O$_{4c}$

vacancy defective Zn$_2$Ga$_2$O$_4$ (100), (110), and (111) surfaces. Structures of the

transition states (TS1-4) are shown beside the potential energy profiles, respectively. See Figures 3 for color coding.

activation barrier of 0.62 eV. In TS1, the distance between C and Zn_{2c} increased to 2.40 Å from 2.32 Å in the (**100-Vo$_{3c}$-mol**) configuration, the angle of CO_2 was 108.7°, and the C–O_a and C-O_b bond lengths were 1.20 Å and 2.02 Å, respectively. Moreover, because the product (**100-Vo$_{3c}$-dis**) was more stable than the reactant (**100-Vo$_{3c}$-mol**) (0.06 eV higher), the decomposition of CO_2 on the (**100)-Vo$_{3c}$** surface would be exothermic. For the other three defective surfaces, only the molecular adsorption state on the (**110)-Vo$_{3c}$** surface was exothermic (i.e., the (**100-Vo$_{3c}$-mol**) state was more stable than the free CO_2 + slab), and the other two states on the (**111)-Vo$_{3c}$** and (**111)-Vo$_{4c}$** surfaces were both endothermic. This suggests that spontaneous molecular adsorption on the defective (111) surface is difficult. In contrast to the situation on the (**100)-Vo$_{3c}$** surface, all of the products on these three surfaces were less stable than the reactants, so the decomposition of CO_2 on them would be endothermic. In addition, comparison of the results of the potential energy profiles in Figure 6 shows that the lowest energy barrier (0.62 eV) and reaction energy (-0.06 eV) were both found on the (**100)-Vo$_{3c}$** surface, whereas the highest energy barrier (5.02 eV) and reaction energy (1.24 eV) were both found on the (**111)-Vo$_{3c}$** surface. This provides further kinetics-based proof of our conclusions that the (**100)-Vo$_{3c}$** surface would be the best surface for CO_2 decomposition and that the activity of these surfaces decreases in the order (**100)-Vo$_{3c}$** > (**110)-Vo$_{3c}$** > (**111)-Vo$_{4c}$** > (**111)-Vo$_{3c}$**. Therefore, if we want to synthesize a $ZnGa_2O_4$ catalyst for CO_2 decomposition, we should let the catalyst

expose more (100) surface and generate more oxygen vacancy defects on it.

3.3. CO_2 Adsorption on the Hydrated Perfect (100), (110), and (111) Surfaces.

After considering the various possible initial structures, we obtained the most stable

structure for each surface, as shown in Figure 7. In this simulation, the hydrated

(100-Hy, Zn-Ga-d)
E(t)= -0.09 eV
E(CO_2)= -0.19 eV

(110-Hy, Zn-c)
E(t)= -0.03 eV
E(CO_2)= 0.20 eV

(111-Hy, Zn-c)
E(t)= -0.06 eV
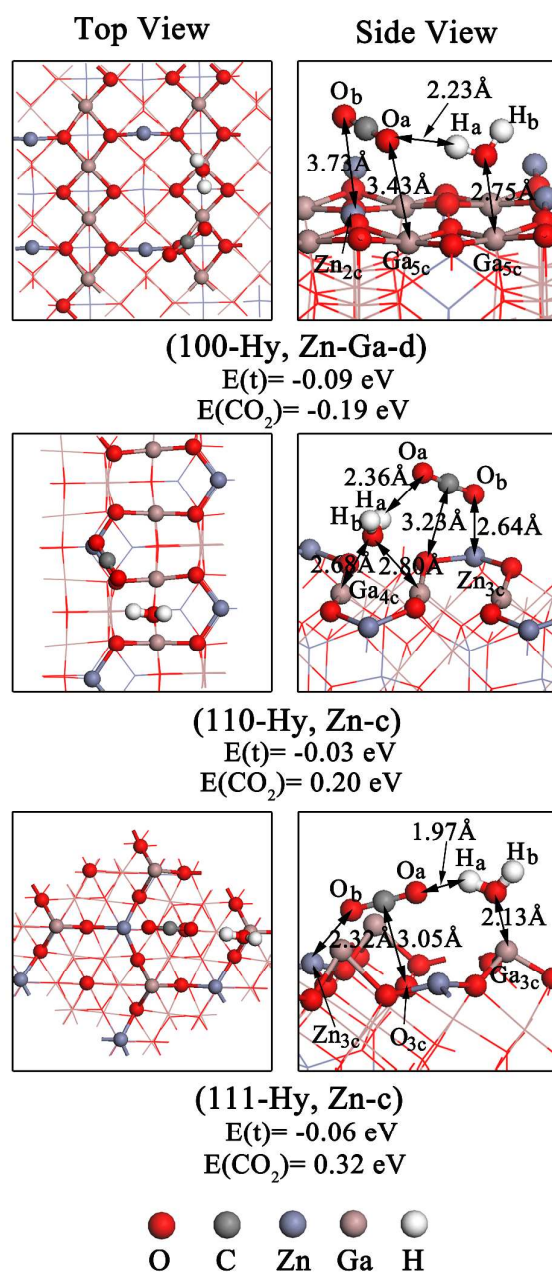E(CO_2)= 0.32 eV

O　C　Zn　Ga　H

Figure 7. Top (left) and side (right) views of the most stable CO_2 adsorption structures

and energies on the hydrated perfect $ZnGa_2O_4$ (100), (110), and (111) surfaces. E(t):

the total adsorption energies of the CO_2 and H_2O; $E(CO_2)$: the adsorption energies of

the CO_2, which is defined as $E(t)-E(H_2O)$ ($E(H_2O)$ is shown in Figure S8).

surfaces were created by adsorbing water molecules on the perfect $ZnGa_2O_4$ surfaces.

The adsorption energy and structure for each hydrated perfect surface are provided in

Figure S8. Comparing the three adsorption energies of CO_2 ($E(CO_2)$ in Figure 7), we

find that the most stable states are on the (100) surface in this case, as well. Moreover,

the presence of the coadsorbed H_2O on these three surfaces makes the overall

adsorption process more thermodynamically favorable than that on the clean surfaces

(seen in Table 1). This can be explained by the special structures of the coadsorbed

states. In Figure 7, the distances between the hydrogen atoms (H_a) of the adsorbed

H_2O molecules and the oxygen atoms (O_a) of the CO_2 molecules were 2.23 Å, 2.36 Å,

and 1.97 Å, respectively, which are small enough to generate hydrogen bonds (less

than 2.50 Å). Therefore, hydration enhances the stability of the CO_2 adsorption states.

Next, we compared CO_2 adsorption on the dry defective $ZnGa_2O_4$ surfaces with

that on the hydrated perfect $ZnGa_2O_4$ surfaces to help clarify which surface

modification had a greater effect on CO_2 adsorption and activation. Although

protonation of the adsorbed CO_2 made the overall adsorption process

thermodynamically favorable, the changes in the CO_2 adsorption energies on the

(100), (110), and (111) surfaces were very small (0.03 eV, 0.02 eV, and 0.03 eV,

respectively). On the other hand, the most stable CO_2 molecular adsorption states on

the dry defective surface in the **(100-Vo$_{3c}$-mol)**, **(110-Vo$_{3c}$-mol)**, and **(111-Vo$_{4c}$-mol)**

configurations had adsorption energies of -0.74eV, -0.43 eV, and 0.20 eV, respectively,

which were much more stable than the adsorption states on clean surfaces. Therefore, surface oxygen defects enhanced the CO_2 adsorption much more than hydration. To further examine the effect of the preadsorbed water on CO_2 adsorption on the defective surfaces, we calculated CO_2 adsorption behavior on the hydrated defective surfaces as well.

3.4. CO_2 Adsorption and Dissociation on the Hydrated (100), (110), and (111) Surfaces with Oxygen Vacancy Defects. In this section, we calculate the stability of CO_2 adsorption on the hydrated defective surfaces with oxygen vacancies, as well as the effect of water on CO_2 adsorption on the defective surfaces. Because the stable adsorption states all involved the vacancy defect sites, we mainly discuss the changes in the molecular and dissociative adsorption behaviors on these sites. Furthermore, our calculations also indicated that the adsorption behaviors on the other sites were similar to those on the hydrated perfect surfaces. The adsorption energy and structure for each hydrated defective surface are provided in Figure S9.

For the (100) surface, the coadsorption of CO_2 and H_2O would significantly enhance the stability of the adsorption state, especially for the **(100-Vo$_{3c}$-Hy-mol)** state, as shown in Figure 8. This can be explained by the specific structure of the **(100-Vo$_{3c}$-Hy-mol)** state. In the **(100-Vo$_{3c}$-Hy-mol)** state, the length of the H$_a$–O$_a$ hydrogen bond is 1.81 Å, which is much shorter than the hydrogen bond in **(100-Vo$_{3c}$-Hy-dis)** (2.26 Å). This means that the interactions between the H$_a$ and O$_a$ atoms in the **(100-Vo$_{3c}$-Hy-mol)** state are much stronger than in the **(100-Vo$_{3c}$-Hy-dis)**. This suggests that the strength of the hydrogen bond will play an

20

Top View   Side View   Top View   Side View

(100-Vo3c-Hy-mol)
E(t)= -1.41 eV
E(CO$_2$)=- 0.99 eV

(100-Vo3c-Hy-dis)
E(t)= -1.28 eV
E(CO$_2$)=- 0.86 eV

(110-Vo3c-Hy-mol)
E(t)=- 0.78 eV
E(CO$_2$)= -0.57 eV

(110-Vo3c-Hy-dis)
E(t)=- 0.10 eV
E(CO$_2$)= 0.11 eV

(111-Vo3c-Hy-mol)
E(t)= 0.47 eV
E(CO$_2$)= 0.78 eV

(111-Vo3c-Hy-dis)
E(t)= 1.77 eV
E(CO$_2$)= 2.08 eV

(111-Vo4c-Hy-mol)
E(t)=- 0.45 eV
E(CO$_2$)= 0.04 eV

(111-Vo4c-Hy-dis)
E(t)= 0.47eV
E(CO$_2$)= 0.85 eV

O   C   Zn   Ga   H
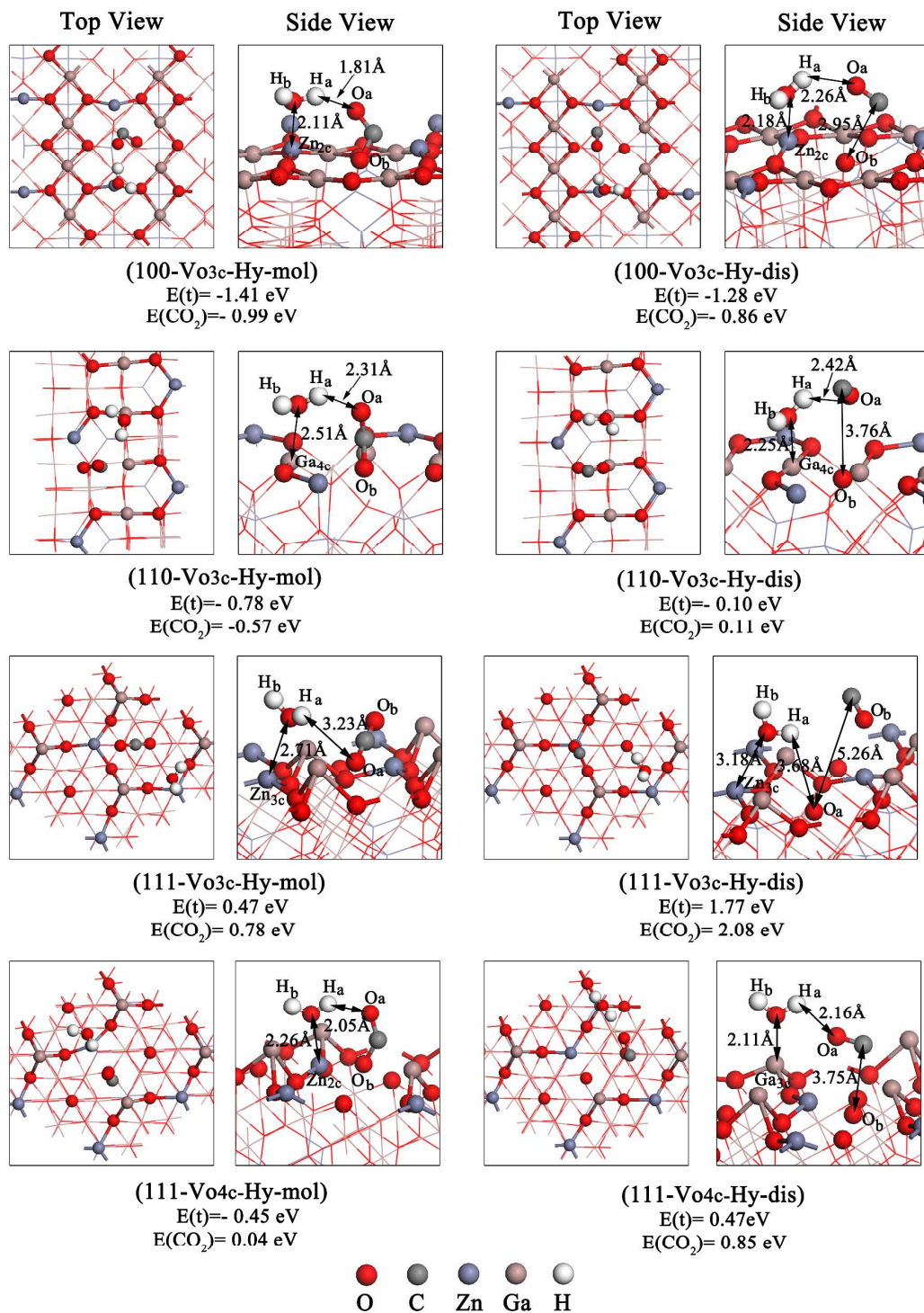
Figure 8. Top (left) and side (right) views of the CO$_2$ molecular and dissociation adsorption structures and energies on the oxygen vacancy sites of the hydrated defective ZnGa$_2$O$_4$ (100), (110), and (111) surfaces. E(t): the total adsorption energies

21

of the CO_2 and H_2O; $E(CO_2)$: the adsorption energies of the CO_2, which is defined as

$E(t)-E(H_2O)$ ($E(H_2O)$ is shown in Figure S9).

important role in the stability of the coadsorption state. As was the case for the dry

Vo_{4c} defective (100) surface, the CO_2 adsorption states on the hydrated (100) surface

with Vo_{4c} defects were quite unstable. In particular, our calculations indicate that the

H_2O and CO_2 coadsorption could not happen on the Vo_{4c} defect site, and the H_2O and

CO_2 molecules had a tendency to remain far away from the surface rather than

adsorbing onto it. This implies that spontaneous coadsorption on the Vo_{4c} defective

site is impossible.

In our previous work,[45] we pointed out that the oxygen vacancies were also good

sites for H_2O adsorption and decomposition and that the dissociation adsorption

energy of H_2O on the defective (100) surface is -0.79 eV, which is similar to the

dissociation adsorption energy of CO_2 on the hydrated defective (100) surface (-0.86

eV). Therefore, hydration would compete with CO_2 adsorption and decomposition for

the oxygen vacancy sites if both H_2O and CO_2 were present in the gas phase.

Comparing the adsorption energies for CO_2 ($E(CO_2)$) in Figure 6, we further find that

the molecular absorption (reactant) on the **(100-Vo$_{3c}$-Hy)** surface is more favorable

thermodynamically. This would make the decomposition of CO_2 on the **(100-Vo$_{3c}$-Hy)**

surface endothermic, which is disadvantageous for the decomposition of CO_2.

Moreover, the transition states for dissociative adsorption on the hydrated defective

(100) surface also show that the coadsorption of H_2O increases the energy barrier for

the decomposition of CO_2, as shown in Figure 9. This provides further kinetics-based

proof for our conclusion that the hydrated defective (100) surface is not good for CO_2

decomposition, as compared to the dry defective (100) surface.

Next, for the **(110)-Vo$_{3c}$** and **(111)-Vo$_{4c}$** surfaces, the generation of hydrogen bonds

between H_a and O_a could enhance the stability of the adsorption states, as well.

However, because the molecular adsorption and dissociative adsorption of H_2O[45] are

much more stable than the adsorption of CO_2, there would be significant competition

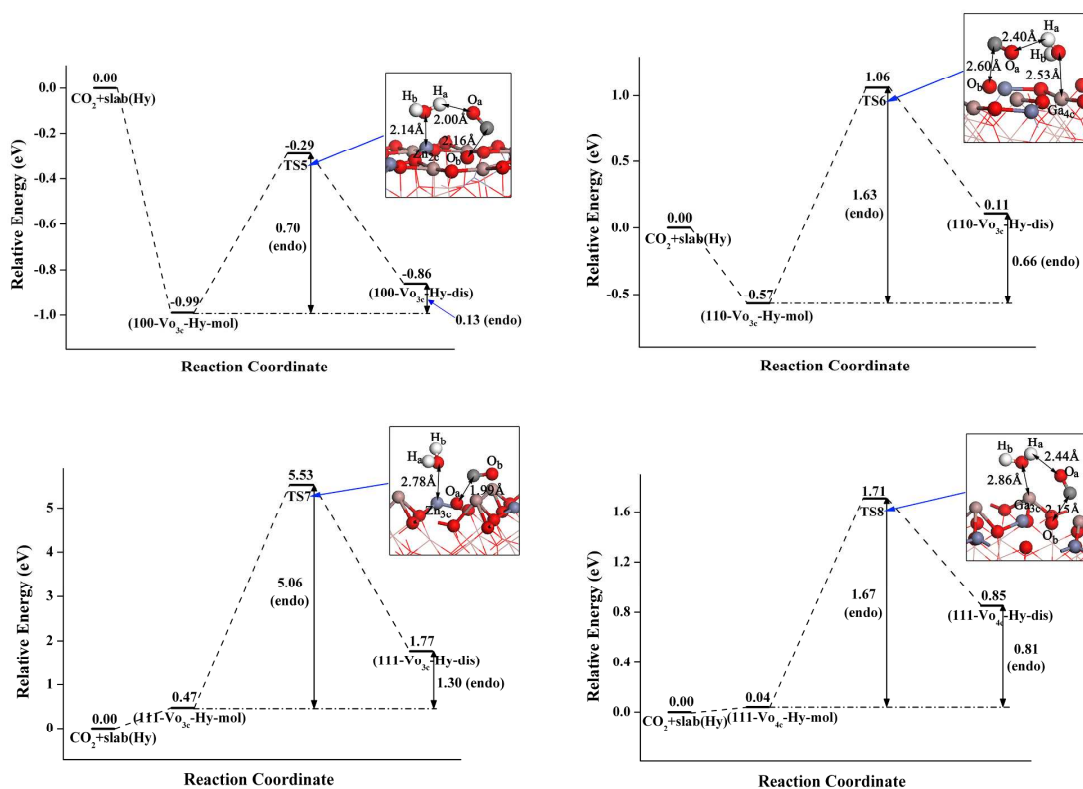between H_2O and CO_2 for the vacancy sites, which is quite disadvantageous for the

Figure 9. Potential energy profiles for the dissociation of CO_2 on the hydrated O_{3c} or

O_{4c} vacancy defective $Zn_2Ga_2O_4$ (100), (110), and (111) surfaces. Structures of the

transition states (TS7 and TS8) are shown beside the potential energy profiles,

respectively. See Figures 7 for color coding.

23

decomposition of CO_2. Moreover, the transition states shown in Figure 9 also indicate that the coadsorption of H_2O could increase the energy barriers of the decomposition of CO_2 on these two surfaces and make them even more kinetically unfavorable. Finally, for the **(111)-Vo$_{3c}$** surface, unlike for the other surfaces, the coadsorption of H_2O even made the CO_2 molecular adsorption and dissociative adsorption states less stable than on the dry defective surface, in addition to increasing the energy barrier for the decomposition reaction (seen in Figure 9). The CO_2 molecular adsorption and dissociative adsorption configurations in Figure 8 show that the distances between H_a and O_a were 3.23 Å and 3.68 Å, respectively, which were too long to generate hydrogen bonds. This further confirms our conclusion that the generation of a hydrogen bond was the key factor that made the coadsorption state more stable than on the dry surfaces.

Thus, it was found that the coadsorption of H_2O can enhance the stability of the CO_2 adsorption state on defective $ZnGa_2O_4$ surfaces (except for the **(111)-Vo$_{3c}$** surface). However, because the oxygen vacancy defects can also adsorb H_2O molecules (on some surfaces, the adsorption states of H_2O are much more stable than the adsorption states of the CO_2), there will be strong competition between them. Therefore, the presence of H_2O will decrease the availability of surface oxygen vacancy sites for CO_2 activation and decomposition. Combining this competition with the kinetic effects (the coadsorption of H_2O can increase the energy barrier for the decomposition of CO_2), we can conclude that the presence of water will have a negative effect on the catalytic activity of $ZnGa_2O_4$ catalysts toward CO_2 conversion.

Therefore, if we want to use $ZnGa_2O_4$ catalyze CO_2 decomposition into CO and O_2, we should be sure that the reaction system is in a dry environment. Furthermore, if we want to use $ZnGa_2O_4$ to catalyze the reaction between CO_2 and H_2O yielding hydrocarbons, we need to separate and remove water from the product stream to maintain the high activity of the catalysts.

4. CONCLUSIONS

In the present work, the effect of water and oxygen vacancies on CO_2 adsorption on the low-index $ZnGa_2O_4$ (100), (110), and (111) surfaces has been studied using DFT slab calculations. The results show that CO_2 adsorption on the low-index $ZnGa_2O_4$ surfaces is a structure-sensitive reaction and that the surface atomic and electronic structure, oxygen vacancies, and hydration all play important roles in the reaction parameters. On the dry perfect surface, only the CO_2 molecular adsorption on the (100) surface was exothermic and thermodynamically favorable. The dry perfect surface showed CO_2 activation ability, but dissociative adsorption could not proceed.

A defective $ZnGa_2O_4$ surface was created by removing a surface O_{3c} or O_{4c} atom from the dry perfect surface. We found that the presence of oxygen vacancies could promote CO_2 activation and decomposition on the low-index $ZnGa_2O_4$ (100), (110), and (111) surfaces. The oxygen vacancy sites also provided active sites for CO_2 decomposition, and the most stable dissociative adsorption state involved the **(100)-Vo$_{3c}$** surface. Accordingly, a high oxygen vacancy density should improve the CO_2 adsorption and activation and, thereby, improve the catalytic activity of $ZnGa_2O_4$

catalysts for CO_2 conversion. Our results also indicate that because of the generation of hydrogen bonds, the coadsorption of H_2O and CO_2 could enhance the stability of the adsorption state (except the **(111)-Vo$_{3c}$** surface). However, the coadsorption of H_2O would increase the energy barrier for the decomposition of CO_2. Furthermore, because the oxygen vacancy defects also show good activity for H_2O adsorption and decomposition, the H_2O molecules would compete with CO_2 molecules for the oxygen vacancy sites. Therefore, if we want to synthesize a $ZnGa_2O_4$ catalyst for CO_2 conversion, we need to expose the (100) surface more than the other surfaces and generate more vacancy defects. In addition, separating and removing water from the product stream will help to maintain high activity of $ZnGa_2O_4$ catalysts.

Supporting Information

The structures and energies of the less stable states on the (100), (110), and (111) surfaces, the top views of the optimized structures of the defective $ZnGa_2O_4$ (100), (110) and (111) surfaces, CO_2 adsorption structures and energies on the vacancy defective $ZnGa_2O_4$ (110) and (111) surfaces, the adsorption structures and energies of H_2O on the perfect and defective (100), (110), and (111) surfaces, the molecular and dissociative adsorption structures and energies of H_2O on the oxygen vacancy sites of the (100), (110), and (111) surfaces. This material is available free of charge via the Internet at http://pubs.acs.org.

Acknowledgment

References

(1) J. Houghton, *Rep. Prog. Phys.*, 2005, **68**, 1343 −1403.

(2) T. R. Karl and K. E. Trenberth, *Science*, 2003, **302**, 1719 −1723.

(3) L. V. Heisey, *J. Chem. Educ.*, 1977, **54**, A130−A131.

(4) D. Preti, C. Resta, S. Squarcialupi and G. Fachinetti, *Angew. Chem., Int. Ed.*, 2011, **50**, 12551 −12554.

(5) C. S. Yoo, *Phys. Chem. Chem. Phys.,* 2013, **15**, 7949−7966.

(6) V. P. Indrakanti, J. D. Kubicki and H. H. Schobert, *Energy Environ. Sci.*, 2009, **2**, 745 −758.

(7) K. H. Ernst and D. Schlatterbeck, *Phys. Chem. Chem. Phys.*, 1999, **1**, 4105−4112.

(8) M. Behrens, F. Studt, I. Kasatkin, S. Kühl, M. Ha ̈vecker, F.Abild-Pedersen, S. Zander, F. Girgsdies, P. Kurr and B.-L. Kniep, et al. *Science*, 2012, **336**, 893 − 897.

(9) Q. Liu, Y. Zhou, J. H. Kou, X. Y. Chen, Z. P. Tian, J. Gao, S. C. Yan and Z. G. Zou, *J. Am. Chem. Soc.*, 2010, **132**, 14385−14387.

(10) J. Raskó and F. Solymosi, *J. Phys. Chem.*, 1994, **98**, 7147−7152.

(11) O. Seiferth, K. Wolter, H. Kuhlenbeck and H. J. Freund, *Surf. Sci.*, 2002, **505**, 215−224.

(12) Y. Wang, A. Lafosse and K. Jacobi, *J. Phys. Chem. B.*, 2002, **106**, 5476−5482.

(13) T. Inoue, S. Fujishima, S. Konishi and K. Honda, *Nature*, 1979, **277**, 637−638.

(14) H. S. Taylor, *Proc. R. Soc. London, Ser. A*, 1925, **108**, 105−111.

(15) J. K. Nørskov, T. Bligaard, B. Hvolbæk, F. Abild-Pedersen, I. Chorkendorff and

C. H. Christensen, *Chem. Soc. Rev.*, 2008, **37**, 2163−2171.

(16) J. T. Yates, *J. Vac. Sci. Technol. A*, 1995, **13**, 1359−1367.

(17) K. Wandelt, *Surf. Sci.*, 1991, **251- 252**, 387−395.

(18) G. Rupprechter, *Adv. Catal.*, 2007, **51**, 133−263.

(19) Y. X. Pan, C. J. Liu, D. H. Mei and Q. F. Ge, *Langmuir*, 2010, **26**, 5551−5558.

(20) R. T. Vang, K. Honkala, S. Dahl, E. K. Vestergaard, J. Schnadt, E. Laegsgaard, B.

S. Clausen, J. K. Nørskov and F. Besenbacher, *Nat. Mater.*, 2005, **4**, 160−162.

(21) L. J. Liu, F. Gao, H. L. Zhao and Y. Li, *Appl. Catal., B.*, 2013, **134-135**, 349−358.

(22) Y. G. Wang, B. Li, C. L. Zhang, L. F. Cui, S. F. Kang, X. Li and L. Zhou, H. *Appl.
Catal., B.*, 2013, **130-131**, 277−284.

(23) D. D. Sui, X. H. Yin, H. Z. Dong, S. Y. Qin, J. S. Chen and W. L. Jiang, *Catal.
Lett.*, 2012, **142**, 1202−1210.

(24) L. J. Liu, C. Y. Zhao and Y. Li, *J. Phys. Chem. C.*, 2012, **116**, 7904−7912.

(25) H. L. Li, Y. G. Lei, Y. Huang, Y. P. Fang, Y. H. Xu, L. Zhu and X. Li, *J. Nat. Gas
Chem.*, 2011, **20**, 145−150.

(26) A. B.Vidal, L. Feria, J. Evans, Y. Takahashi, P. Liu, K. Nakamura, F. Illas and J.
Rodriguez, *J. Phys. Chem. Lett.*, 2012, **3**, 2275−2280.

(27) H. C. Yang, H. Y. Lin, Y. S. Chien, J. C. Wu and H. H. Wu, *Catal. Lett.*, 2009,

131, 381−387.

(28) M. Zhong, Y. B. Li, T. Takero, M. J. Zheng, I. Yamada and J. J. Delaunay, *Nanopart Res.*, 2012, **14,** 804−814.

(29) M. Zhong, Y. B. Li, I. Yamada and J. J. Delaunay, *Nanoscale*, 2012, **4**, 1509−1514.

(30) M. S. Sun, D. Z. Li, W. J. Zhang, Z. X. Chen, H. J. Huang, W. J. Li, H.Y. He and X. Z. Fu, *J. Solid State Chem.*, 2012, **190**, 135−142.

(31) V. B. R. Boppana and R. F. Lobo, *ACS Catal.*, 2011, **1**, 923−928.

(32) W. W. Zhang, J. Y. Zhang, Z. Y. Chen and T. M. Wang, *Catalysis Communications*, 2009, **10**, 1781−1785.

(33) S. C. Yan, S. X. Ouyang, J. Gao, M.;Yang, J. Y. Feng, X. M. Fan, L. J. Wan, Z. S. Li, J. H. Ye, Y. Zhou and Z, G. Zou, *Angew. Chem. Int. Ed.*, 2010, **49**, 6400−6404.

(34) G. C. Wang, L. Jiang, X. Y. Pang, Z. S. Cai, Y. M. Pan, X. Z. Zhao, Y. Morikawa and J. Nakamura, *Surf. Sci.*, 2003, **543**, 118−130.

(35) S. J. Choe, H. J. Kang, D. H. Park and D. S. Huh, Park, J. *Surf. Sci.*, 2001, **181**, 265−276.

(36) S. G. Wang, D. B. Cao, Y. W. Li, J. G. Wang and H. J. Jiao, *J. Phys. Chem. B.*, 2005, **109**, 18956−18963.

(37) A. B. Vidal, L. Feria, J. Evans, Y. Takahashi, P. Liu, K. Nakamura, F. Illas and J. A. Rodriguez, *J. Phys. Chem. Lett.*, 2012, **3**, 2275 − 2280.

(38) D. C. Sorescu, W. A. Al-Saidi and K. D. Jordan, *J. Chem. Phys.*, 2001, **135**, 124701−124716.

(39) M. Segall, P. Lindan, M. Probert, M. Pickard, C. Pickard, P. Hasnip and S. Clark, M. Payne, *J. Phys.: Condens. Matter*, 2002, 14, 2717−2743.

(40) S. J. Clark, M. D. Segall, C. J. Pickard, P. J. Hasnip, M. J. Probert, K. Refson and M. C. Payne, *Z. Kristallogr.*, 2005, **220**, 567−570.

(41) J. P. Perdew, J. A. Chevary, S. H. Vosko, A. K. Jackson, R. M. Pederson, D. J. Singh and C. Fiolhais, *Phys. Rev. B.*, 1992, **46**, 6671−6687.

(42) J. P. Perdew and Y. Wang, *Phys. Rev. B.*, 1992, **45**, 13244−13249.

(43) D. Sanchez-Portal, E. Artacho and J. M. Soler, *Solid State Commun.*, 1995, **95**, 685−690.

(44) X. Gonze, *Phys. Rev. B.*, 1997, **55**, 10337−10354.

(45) C. Y. Jia, W. L. Fan, F. Yang, X. Zhao, H. G. Sun, P. Li and L. Liu, *Langmuir*, 2013, **29**, 7025−7037.

(46) Z. Y. Zhao, Z. S. Li, and Z. G. Zou, *J. Phys. Chem. C.*, 2012, **116**, 7430−7441.

(47) L. J. Liu, H. L. Zhao, J. M. Andino and Y. Li, *ACS Catal.*, 2012, **2**, 1817−1828.

(48) Y. Zhao, B. T. Teng, X. D. Wen, Y. Zhao, L. H. Zhao and M. F. Luo, *Catal. Commun.*, 2012, **27**, 63−68.

(49) L. Liu, W. L. Fan, X. Zhao, H. G. Sun, P. Li, L. M. Sun, *Langmuir*, 2012, **28**, 10415−10424.

Table of Contents
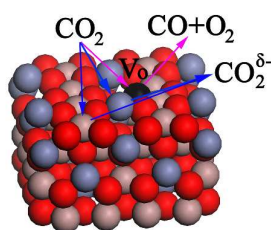
CO_2 adsorption and decomposition on low-index perfect, oxygen vacancy defective, and hydrated $ZnGa_2O_4$ (100), (110) and (111) surfaces were investigate.

The structure sensitivity and the effects of the oxygen vacancy defects and hydration of $ZnGa_2O_4$ catalysts are studied by comparing the adsorption of CO_2 on the perfect, reduced, and hydrated (100), (110), and (111) surfaces of low-index $ZnGa_2O_4$, to gain a theoretical understanding of the CO_2 adsorption on the $ZnGa_2O_4$ surfaces and of the detailed chemistry occurring on its surfaces.